An Experimental Investigation of Steady and Unsteady Combustion Phenomena in the HyShot II Combustor

Stuart J. Laurence[1], Jan Martinez Schramm.[2], Sebastian Karl[3], and Klaus Hannemann[4]
German Aerospace Center (DLR), Göttingen, D 37073, Germany

A series of experiments has been carried out in the HEG facility (High Enthalpy Shock Tunnel, Göttingen) to obtain detailed measurements on the HyShotII scramjet configuration under both steady and unsteady combustion conditions. Standard pressure measurements are performed, but a main focus of this campaign is the use of optical and visualization techniques: high-speed visualizations of OH* chemiluminescence together with pulsed-diode laser Schlieren imaging are employed to gain information about the approximate flame location as well as the interaction between the flow features and combustion characteristics. In particular, this allows an unprecedented level of insight into the transient combustion-induced phenomena present in the combustion chamber at high equivalence ratios. Measurements are compared with computational data obtained from the DLR TAU code.

I. Introduction

TRANSIENT phenomena in scramjet engines are typically associated with unstart of the combustion chamber and inlet[1]. During unstart, the original compression shock system in the inlet is displaced upstream, often resulting in the formation of a detached shock. Unstart can cause violent and unsteady thermal and aerodynamic loads, even leading to the destruction of the engine, and is thus to be avoided in operational scramjet engines. The study of the interacting flow and combustion features leading up to unstart is thus of interest, as it is only through an understanding of these phenomena that unstart can be avoided during scramjet operation. Unstart in supersonic combustion engines is typically caused by one of two factors: (1) excessive heat release in the combustion chamber resulting in the flow becoming subsonic, i.e., thermally choked; (2) the adverse pressure gradient produced by combustion causing the boundary layer to separate, resulting in the formation of an oblique shock train which can propagate upstream. The transient phenomena present during unstart have been the subject of a number of experimental investigations. Many of these[1-3] replace combustion-induced effects with physical blockage, such as pins, plugs or deflecting flaps, which allows the use of cold flows and much simpler implementation of diagnostic techniques such as Schlieren flow visualization. However, while this approach seems reasonable for studying transient flow structures in isolators and inlets, it is inadequate for gaining understanding of the combustion/flow phenomenon leading up to unstart in the combustion chamber itself. Other studies[4,5] have induced unstart by the injection of hydrogen at high equivalence ratios (ER) in model scramjet engines; however, the diagnostics employed in these studies were somewhat limited, resulting in an incomplete picture of the unstart process. In the present study, the transient flow and combustion phenomena produced by the injection of hydrogen at high equivalence ratios were investigated in a reproduction of the HyShot II combustor. The diagnostic tools employed – surface-mounted pressure and heat-flux measurements, pulsed-diode laser Schlieren, and OH* chemiluminescence – allow an unprecedented level of insight into the fluid and combustion phenomena present.

The HyShot II flight experiment of The University of Queensland in Australia[6] was designed to provide benchmark data on supersonic combustion for a flight Mach number of approximately M=8. Extensive ground testing of a 1:1 scale copy of the basic flight geometry has been already carried out[7,8] in the HEG facility (High Enthalpy shock tunnel, Göttingen) of the German Aerospace Agency. In light of the substantial amount of reference data already available for this configuration under both steady and unsteady combustion conditions, it was also chosen as a suitable configuration for the present study.

---

[1] Research Staff, Department of Aerodynamics and Flow Technology, Spacecraft Department
[2] Research Staff, Department of Aerodynamics and Flow Technology, Spacecraft Department.
[3] Research Staff, Department of Aerodynamics and Flow Technology, Spacecraft Department.
[4] Head, Department of Aerodynamics and Flow Technology, Spacecraft Department, AIAA Member.

II. Experimental facility and model

All experiments were carried out in the HEG (High Enthalpy shock tunnel, Göttingen) facility of the German Aerospace Center. The HEG is a reflected-shock tunnel, capable of producing flows over a wide range of stagnation pressures and total enthalpies. A schematic of the facility is shown in Figure 1. Further information on the operating principles and conditions achievable in HEG is provided in Hannemann et al.[9,10]. Briefly, to initiate a test run, compressed air is used to accelerate a free-piston down the compression tube, which is filled typically with a mixture of helium and argon. A primary diaphragm separates the compression tube from the shock tube, containing the test gas: in this case air. When the pressure in front of the piston becomes sufficiently high, the primary diaphragm bursts, sending a strong shock wave down the shock tube. This shock reflects from the far end of the shock tube, bursting the secondary (mylar) diaphragm, which separates the tunnel nozzle and test section, initially under vacuum, from the shock tube. The reflected shock also decelerates the test gas in the shock tube to stagnation conditions, forming the reservoir for the subsequent expansion through the hypersonic nozzle and into the test section. Steady test flow conditions persist typically for several milliseconds; the test time is terminated either by the arrival of the expansion wave from the primary diaphragm burst, or by contamination of the test flow by the driver (compression tube) gas.

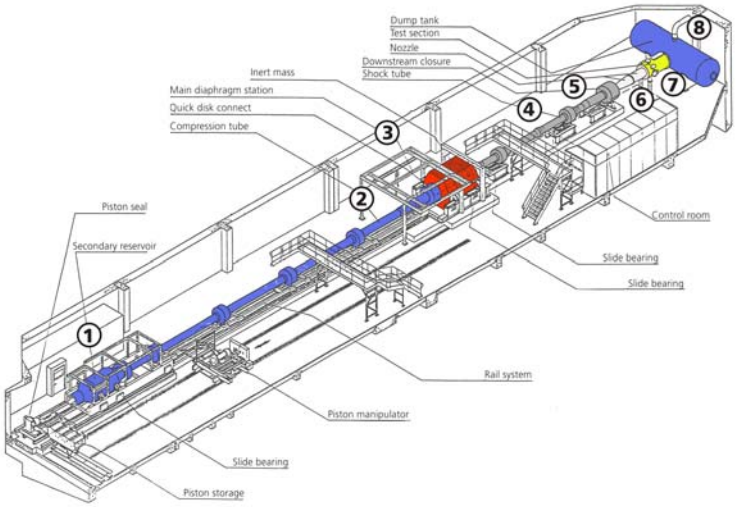

Figure 1: Schematic of the HEG reflected shock-tunnel facility.

For all tests in the current study, HEG Condition XIII (p_0=17 MPa, h_0=3.4 MJ/kg), designed to simulate the flight conditions of the HyShot II vehicle at 28 km altitude, was employed. The free-stream properties corresponding to these stagnation conditions have been calculated computationally (and compared with extensive calibration measurements) as M=7.4, T=270 K, and ρ=0.026 kg/m^3. In Figure 2 are shown reservoir, Pitot and static pressure measurements (the latter two scaled in order to allow a direct comparison) from a typical experiment in the current study. The point t=0 here corresponds to the instant of shock reflection from the shock-tube end wall (this convention is used throughout this paper). A conservative estimate of the steady test time, from 3.5 to 6.0 ms, is indicated by the dashed vertical lines; such a test time was typically chosen for steady combustion cases. However, the flow is established and has achieved roughly constant conditions by 2.5 ms. This point will be important in results discussed later, as some of the relevant unsteady phenomena were observed to be initiated before the onset of the more conservatively chosen test period. Previous experience has shown that comparing the static pressure development to that of the reservoir and Pitot pressures gives a good indication of the arrival of the driver-gas contamination: the Pitot pressure is typically unaffected by driver gas contamination, and follows the reservoir pressure regardless, but the static pressure drops more quickly once driver gas is present in the free stream. In Figure 2, we see that the static pressure development follows that of the reservoir and Pitot pressures until at least 12 ms, indicating that there is no significant contamination during this time. The steady test time is instead terminated by the arrival of expansion waves from the primary-diaphragm burst.

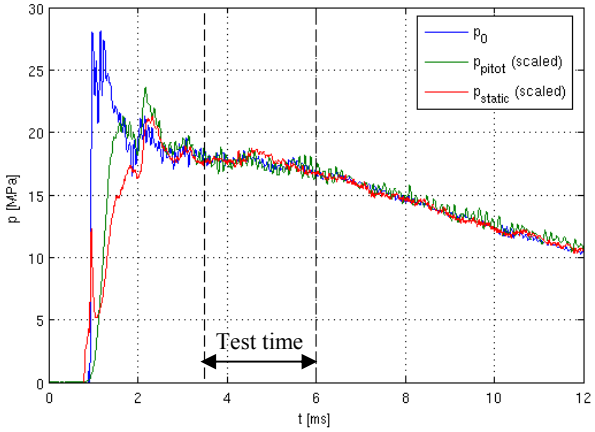

Figure 2: Typical stagnation, Pitot and static pressure traces (the latter two scaled) for an experiment in the current study. The steady test time is indicated by the vertical dashed lines (3.5 to 6 ms).

The HyShot II model used in the present experiments was a modified version of that used in previous experimental campaigns in HEG[7,8]; the modifications were chiefly to improve handling characteristics and optical access. A drawing of the model is shown in Figure 3. The model geometry is a simplified configuration designed to provide reference supersonic combustion data, rather than to produce thrust at the tested conditions. The intake is an 18º ramp, 196 mm wide and 350 mm long, with side walls to ensure the two-dimensionality of the flow entering the combustion chamber. The combustion chamber consists of a constant-area section of length 300 mm, followed by a simple expansion formed by two straight-edged thrust surfaces. The constant-area combustion chamber is 9.8 mm high by 75 mm wide. A boundary-layer bleed channel is employed to prevent the intake boundary-layer from entering the combustion chamber; this also serves to swallow the shock generated at the leading edge of the cowl. Windows were installed both in the intake side-walls and in the combustion chamber side-walls in order to allow flow and OH* visualizations to be obtained. For OH* visualization, quartz windows were employed to allow transmittance of the relevant wavelength (~310 nm). For all experiments, the model was placed at an angle-of-attack of 3.6º (i.e., so that the ramp angle was 21.6º to the free stream).

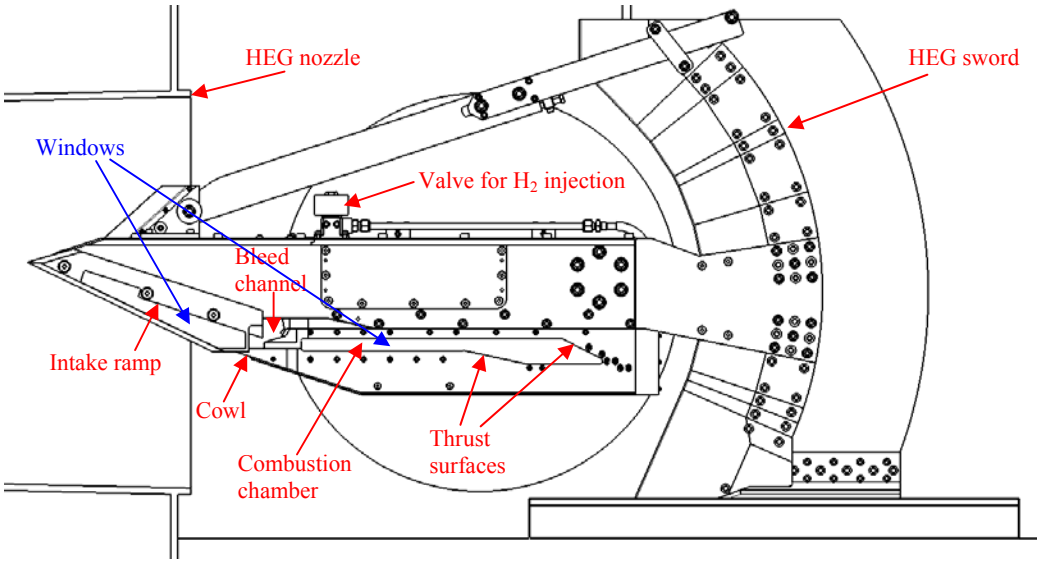

Figure 3: Schematic of the HyShot II model inside the HEG test section.

Hydrogen fuel was injected in the wall-normal direction through four evenly spaced holes on the ramp side of the combustion chamber, at a distance 58 mm downstream from the leading edge of this wall (i.e., from the beginning of the constant area section). The porthole injectors were each of radius 1 mm, providing a total injection

area of 12.6 mm^2. The hydrogen was provided by a Ludwieg tube, capable of providing an approximately constant pulse of fuel for 50 ms at pressures of up to 15 MPa. To ensure the injection was fully established by the arrival of the test flow, injection was triggered in each run approximately 20 ms before the test time by a recoil signal from the compression tube.

III. Measurement techniques

In total, the model was instrumented with 57 pressure transducers and 72 thermocouples, distributed over the inlet ramp, combustion chamber walls and thrust surfaces; it was also equipped with probes to measure the free-stream Pitot and static pressures, and a reference heat-flux value. In the combustion chamber, a single row of pressure transducers was installed on each of the injector- and cowl-side walls, extending out into the thrust nozzle; in each case this was along the symmetry line between two injection port-holes. The transducer type employed was the Kulite XCL-100, with a maximum pressure range of between 170 and 700 kPa (the higher sensitivity models were used on in the expansion nozzle). Thermocouples for the measurement of heat-transfer rates were also installed inside the combustion chamber, but they will not be discussed further in this paper.

One of the main focuses of the current experiments was to obtain visualizations of OH* chemiluminescence within the combustion chamber. OH* chemiluminescence, being an integrated line-of-sight quantity, is limited in its ability to provide quantitative measurements in three-dimensional flow-fields such as the present one. However, the effective integration that takes place may be reproduced computationally; thus, these measurements are suitable as a further verification for computational simulations of combusting flow-fields. In hydrocarbon flames, it has been shown[11] that OH* is not an adequate indicator of heat release. However, other authors[12] have recommended OH* chemiluminescence as an attractive option where other, especially laser-based, techniques would be difficult to apply; indeed, in a facility such as HEG, the implementation of OH PLIF imaging would entail a significantly greater level of difficulty than the present measurements.

For these experiments, the OH* visualization apparatus consisted of a Shimadzu HPV-1 high-speed camera used in conjunction with a LaVision HS-IRO intensifier. Both the model combustor sidewalls and the HEG test section were fitted with quartz windows to allow transmittance of the relevant wavelength (310nm), and a custom band-pass filter (of 50nm width centered at 310nm) was placed in front of the intensifier to block both other flame emissions and the considerable self-luminosity produced by the HEG facility. For steady combustion tests at ER=0.35, images were captured at 8 kfps, with a integration time for the IRO of 60 μs; for the higher equivalence ratios, the more intense combustion allowed a shorter exposure time of 10 μs together with a camera frame rate of 16 kfps. With this latter combination, the study of unsteady phenomena in the combustion chamber was possible.

Schlieren imaging was also employed to study the fluid structures within the combustion chamber. Employing such flow imaging techniques in a combusting environment can be challenging because of the intense luminosity produced by combustion. The use of a monochromatic light source, such as a laser, can overcome this problem, as a narrow band-pass filter can be installed in the light-path after the test section, removing most of the luminosity. Lasers typically also provide light pulses of very short duration, allowing the visualized structures to be effectively frozen in time. However, the use of coherent light for visualization also has serious drawbacks, most notably the appearance of strong diffraction fringes in images. An ideal light source for the present experiments would thus provide decoherent, monochromatic pulses of short duration; fortunately, such a source has recently become available and was employed in these experiments. The Cavilux Smart is a pulsed-diode laser designed specifically for visualization purposes. It produces pulses at 690 nm of duration as short as 10 ns and at repeat rates of up to 100 kHz (or higher for a very short total duration, using a special ultra-high speed mode). For the current experiments, a standard Z-fold Schlieren setup was employed with the laser as the light source, with images captured by the Shimadzu HPV-1 camera. Typical frame rates were 16 or 32 kHz, and light pulses of 30 ns duration were employed.

The advantages of employing the Cavilux laser as a light source over the use of a continuous source (especially with the Shimadzu camera, for which the minimum framing time is 1/8 of the time between images) is demonstrated in Figure 4. Both images show the flow structures directly downstream of the hydrogen injector at a high equivalence ratio (approximately 0.7). Note that both images have been flipped in the vertical direction (as are all subsequent images in this paper), since earlier work employing the HyShot II combustor had the model turned upside-down compared to the present configuration. The upper image was captured using a 1000W Xenon short-arc continuous white-light source (with a framing time controlled by the camera of 16 μs), while the lower image was produced with the laser. While the shock structures are visible in both images (the high power of the continuous source meant that neutral density filters could be employed to remove the combustion-induced luminosity), they are significantly sharper in the lower image, and the turbulent flow structures produced by injection are also visible.

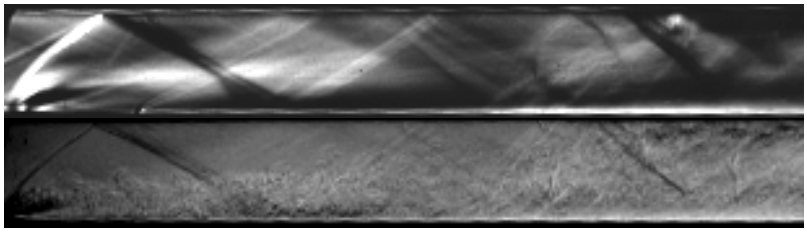

Figure 4: Schlieren visualizations of flow near injector with ER=0.7, captured using a continuous light source (above) and a pulsed-diode laser (below)

Note that because of the availability of only a single camera, OH* and Schlieren images could not both be captured during the same experiment. This, if unsteady data were to be compared between shots, the timescales had to be synchronized through means of the surface-mounted transducers, as outline in section V.

IV. Steady supersonic combustion data

Steady supersonic combustion data was obtained for a nominal equivalence ratio of ER=0.35. A number of shots were carried out at this equivalence ratio, both to ensure repeatability and to enable the visualization of various parts of the combustion chamber. One of the disadvantages of the Shimadzu HPV-1 is a relatively low resolution (312x260 pixels), which means to obtain sufficiently resolved images of the long, narrow HyShot II combustion chamber, it had to be imaged in sections. In Figure 4 are shown visualizations of the various parts of the combustor under steady combustion conditions. The images of the intake ramp and rear thrust surface were obtained using the continuous 1000W white-light source mentioned above, while the three images of the combustion chamber used the pulsed-diode laser light source.

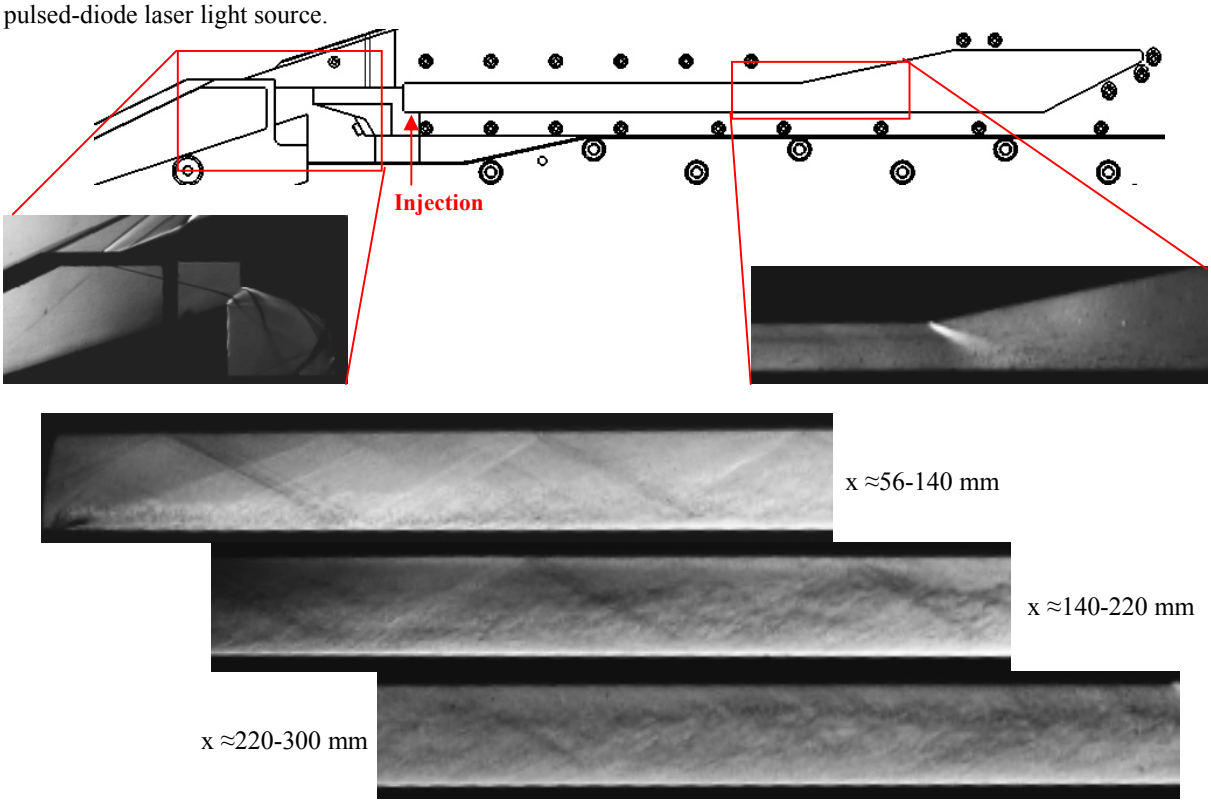

Figure 5: Visualizations of various sections of the HyShot II model (shown upside down relative to wind-tunnel configuration) under steady supersonic combustion conditions: ER=0.35, α=3.6°. The lower three images show, respectively, the front, center, and rear thirds of the constant-area combustion chamber downstream of the injection point.

The intake visualization of Figure 5 shows the cowl shock being swallowed by the boundary-layer bleed channel, as intended in the design. Inside the combustion chamber, the shock train produced by the bow-shock at the injection point is clearly visible in the first two sections; by the rear section it has become almost invisible, but that the flow is still substantially supersonic at the end of combustor is clear from the expansion fan visible in the visualization of the cowl-side thrust surface. The injected hydrogen is also visible, from both the turbulent structures created and the density jump at the interface with the incoming air stream. By the end of the combustor, the penetration depth of the hydrogen is seen to be approximately 75% of the combustor height.

In figure 6 is shown an averaged composite Schlieren/OH* visualization (in each case constructed by averaging all images obtained over the steady test time). The combustion features indicated by the presence of OH* are seen to be clearly related to the flow structures in the duct: in particular, the first reflection of the injection shock is seen to initiate combustion close to the injector-side wall; the second reflection "kicks" the flame further out into the duct, increasing the level of combustion taking place.

Figure 6: Composite OH* chemiluminescence and Schlieren images near the injector for steady supersonic combustion (ER=0.35) superimposed on one another

Figure 7 shows mean pressure profiles on the injector side wall for three experiments with the same nominal equivalence ratio of 0.35. The pressure values are normalized by the reservoir pressure to allow direct comparison with computational results. The error bars indicate the level of unsteadiness in each pressure measurement during the test time, in this case showing the 95% confidence level. The level of repeatability in the experimental measurements is seen to be good, with most points lying very close to one another. The steady rise in static pressure observed is indicative of supersonic combustion occurring down the length of the duct. Also shown is a computational pressure profile obtained using the TAU code[13] for an equivalence ratio of 0.355. This computation was performed using the Spalart-Allmaras turbulence model, Schmidt numbers of 0.7 and a non-catalytic wall boundary condition. Agreement between experiment and CFD in the second half of the duct and into the expansion is good, but there are some discrepancies in the first section of the duct. The may be a result of both inadequate grid resolution in the CFD and the slightly different momentum flux ratios in the experiments and CFD (due to slightly differing reservoir conditions), which would have an effect on, in particular, the exact location of the shock train. It is also clear from the strong peaks in the computational profile that the pressure reading is very sensitive to the exact location of each of the shocks in the shock train.

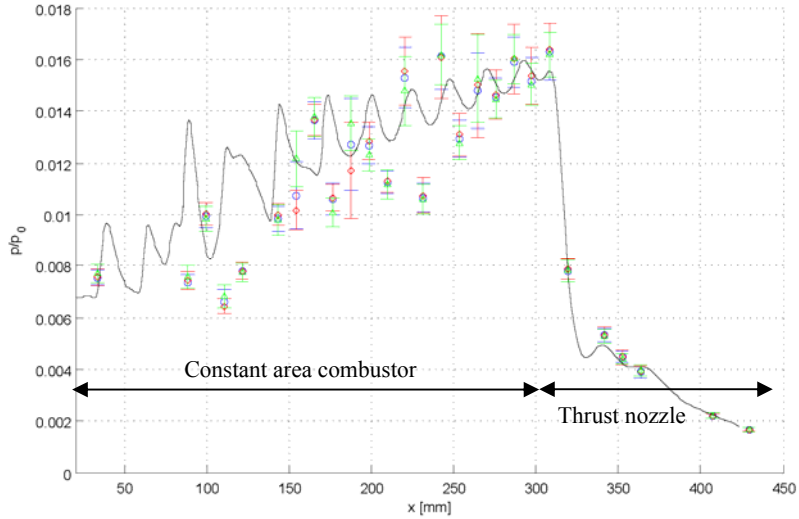

Figure 7: Pressure profile on the injector-side wall for steady supersonic combustion at ER=0.35. Results from three experiments are shown together with that from a TAU computation (ER=0.355)

V. Unsteady and choked combustion data

As described in the introduction, as the equivalence ratio is increased in a supersonic combustor, the increased heat release and pressure can lead to one of two operational limits: thermal choking or boundary-layer separation. Thermal choking occurs when the heat release is sufficient to cause the flow to become subsonic within the combustor: in this case, no further heat can be added and the flow topology must undergo a qualitative change in order to accommodate the additional heat release, typically through unstart of the inlet (this is the only possible solution in the idealized zero-dimensional case of Rayleigh flow). Alternatively, if the adverse pressure gradient is sufficiently high at some point in the combustor, separation of the boundary-layer occurs, leading to the formation of an oblique shock train with a supersonic core. Practical dual-mode scramjet/ramjet engines are equipped with a constant area isolator in order to contain the oblique shock train and prevent unstart of the inlet.

In either case, transient flow phenomena will be induced within the combustor; one of the chief aims of the present study was to gain a better understanding of the unsteady processes that develop at high equivalence ratios in the present configuration. Earlier experiments with the HyShot II combustor in HEG showed that, for equivalence ratios above approximately 0.45, a sharp pressure peak develops towards the rear of the combustor and propagates upstream at a velocity that depends to some extent on the equivalence ratio. In the present experiments, unsteady data was obtained for equivalence ratios of approximately 0.5, 0.7, and 1.1. In figure 9 are shown mean pressure values on the injector side wall at 0.4 ms intervals during experiments with each of these equivalence ratios. The error bar for each measurement shows the standard deviation in the pressure during the relevant 0.4 ms period. For each equivalence ratio, the propagation of a sharp pressure rise upstream is clearly observed. The plateau in the measured pressure downstream of the sharp rise suggests that combustion is subsonic in this region. For ER=1.10, the upstream motion is already underway at the earliest time shown of 2.6 ms, with the beginning of the pressure rise located at approximately x=100mm at this instant. The large standard deviation in the pressure measurements in the initial rise is due to the oscillatory nature of the pressure readings near the initial rise, which is discussed shortly. By 3.4 ms, the pressure rise has reached the pressure transducer at x=33 mm, ahead of the injection point, and the combustion chamber is shortly thereafter fully choked.

For ER=0.7, a sharp pressure rise is observed near x=200mm at t=2.6 ms, and this again subsequently propagates upstream. A quasi-steady configuration, in which the pressure rise has not yet reached the first pressure transducer, is achieved by t=4.6 ms, but following the conclusion of the test time (t=6 ms), the motion of the shock system is observed to continue upstream (the falling reservoir pressure after the test time means that the effective equivalence ratio rises) and the entire combustor eventually unstarts, as in the higher ER case. For the lowest equivalence ratio of 0.53, the development of the transient phenomena occur at later times and further downstream than either of the other two cases. The steady, nearly monotonic increase in pressure in the downstream direction observed in the first two time snapshots suggests the combustion to be still predominantly supersonic at these times. However, the pressure rise then gradually steepens and the characteristic pressure plateau forms. The flow structures are still in the process of moving upstream at the latest time shown of 5.4 ms.

In figure 9 are shown time-resolved pressure traces as recorded by several pressure transducers on the cowl-side wall for an experiment with ER=0.7. In order to make the individual pressure traces more easily visible, the y-axes have been offset by multiples of 1 bar. In these traces, the initial development of the upstream propagating system is seen to be characterized by a sharp pressure peak followed by several large-amplitude oscillations. Such profiles suggest some form of periodic shock structure. The oscillations reach a maximum amplitude near x=176 mm, but thereafter appear to break down to some extent, and further up the duct only the initial peak of the original shock structure appears to remain.

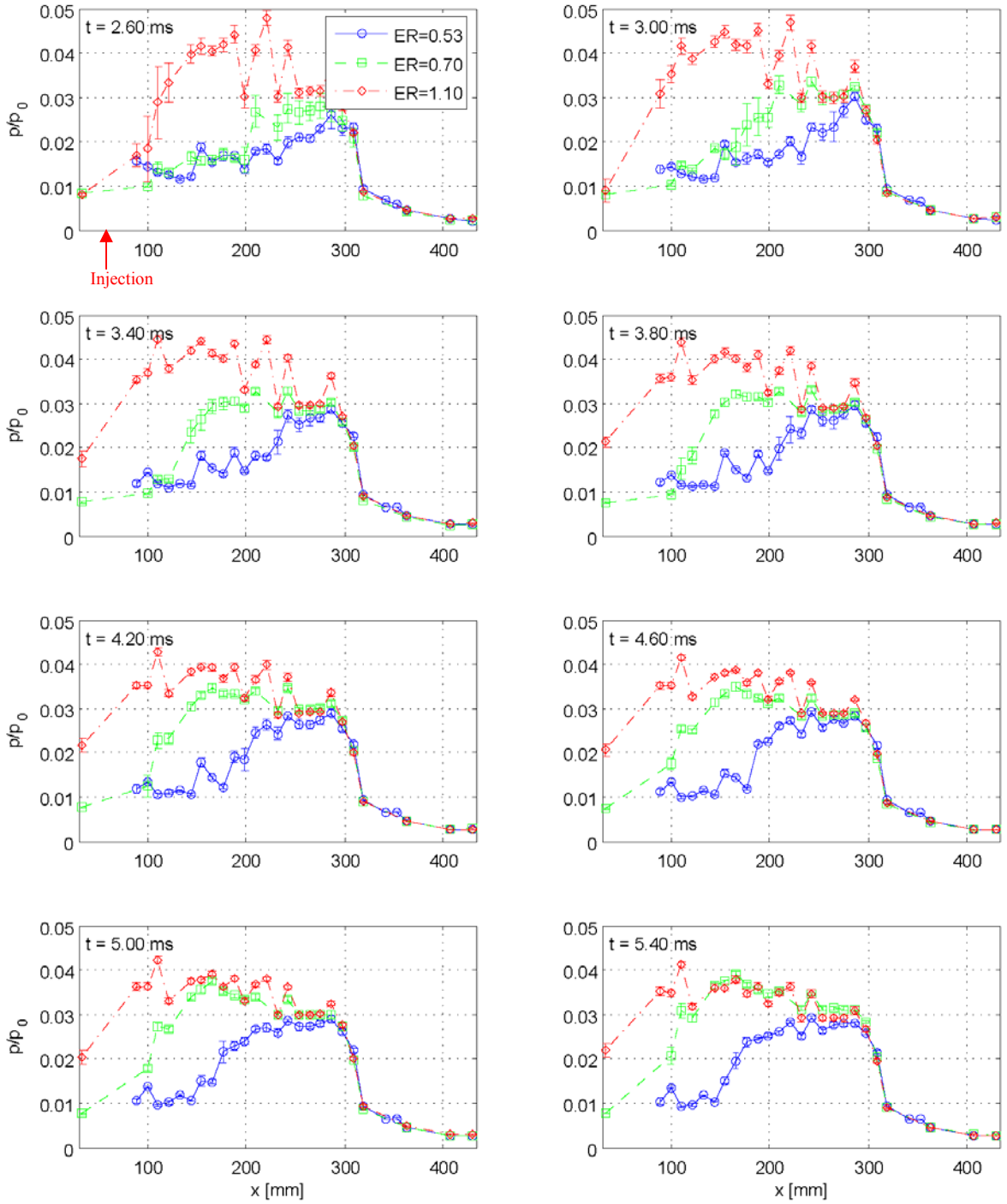

Figure 8: Unsteady pressure development on the injector side wall of the combustion chamber for various supercritical equivalence ratios

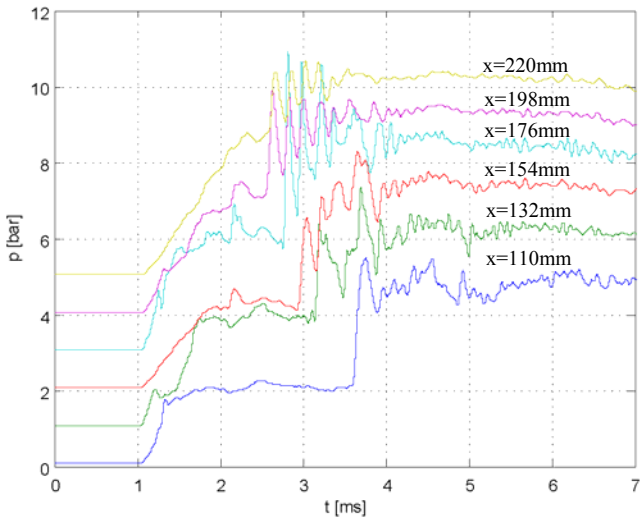

Figure 9: Time-resolved pressure traces at various locations on the cowl-side wall showing the development of periodic structures during the transient phase

In Figure 10 are plotted x-t diagrams showing the motion of the pressure rise upstream on both the injector and cowl sides for all runs with a nominal equivalence ratio of 0.7, determined by the arrival of the rise at each of the pressure transducers. The upstream motion begins before the nominal start of the steady test time (3.5 ms), but, as noted earlier, the flow may be considered to be roughly steady by 2.5 ms (though the higher reservoir pressure at earlier times means that the effective equivalence ratio will be slightly below the nominal value). The speed of propagation is seen to be approximately constant until the structure reaches x≈120mm, at which point it pauses (or, at least, slows down), before once again moving upstream once the test time (6 ms) has concluded. In each plot a line is shown having a slope that corresponds to a propagation velocity of 93 m/s, and this is seen to match well with the propagation speed of structures in the initial part of the development. For ER=0.5, a slower speed of approximately 31 m/s was observed, while for ER=1.1, the speed was typically above 200 m/s (but occurred well before the onset of steady flow).

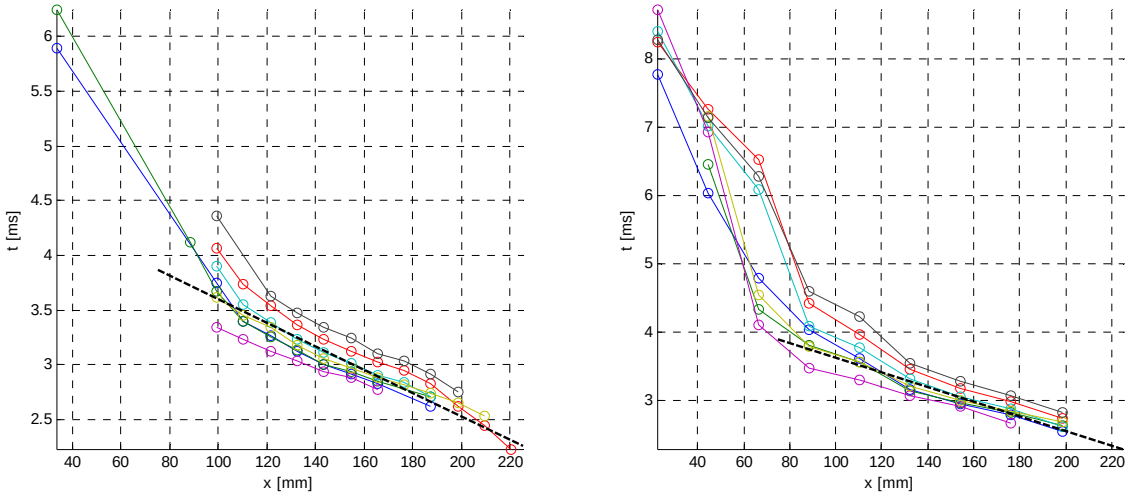

Figure 10: X-t diagrams showing the upstream motion of the unsteady shock system for all shots with an equivalence ratio of 0.7, on the injector side-wall (left) and cowl side-wall (right). The dashed black line in each plot has an inverse slope of 93 m/s.

In order to gain a better understanding of the flow and combustion features present during this unsteady development, high-speed Schlieren and OH* imaging was employed at these high equivalence ratios. Correlating the flow and combustion features between two shots was complicated by the fact that, as mentioned earlier, only one or the other of these techniques could be applied in a given experiment; however, by comparing the motions plotted in figure 10, the relative timescales between experiments could be effectively correlated.

In figure 11, instantaneous composite Schlieren/OH* visualizations (with OH* levels indicated by red coloring) of the flow in the rear-central combustion chamber are shown at different times in experiments with an equivalence ratio of 0.7. Below each image is also plotted the average pressure reading (averaged over a period of 32 μs centered around the visualized instant) for all pressure transducers located within the visualization region (note that the images and plots have been aligned and scaled so that the axial dimensions coincide). The unsteady process appears to commence with the formation of a shock on the cowl-side wall, which then proceeds to propagate upstream. However, it is clear from other visualizations (for example, that at 2.85 ms in figure 10) that the developing shock extends over the height of the combustor; the reason that it is not as clearly visible in the lower half is most likely that the flow is to a large extent subsonic here. From an analysis of the pressure traces, it is also apparent that the pressure rise on the body-side wall also slightly preceded that on the cowl-side wall. This initial shock is seen to then develop into an unsteady shock train that moves up the duct. This explains the strong pressure oscillations observed during the initial transient phase in figure 9; these are also visible in some of the pressure transducer measurements in figure 11 (note, in particular, the injector-side transducer at 176 mm). Regarding the OH* visualizations, some indication of combustion is evident in the second image at 2.63 ms, but there are no strong combustion features associated with the development of the unsteady flow structures; it is not until later images that evidence of substantial combustion is observed. If a separation bubble were to develop on the injector-side wall (where the boundary-layer is most susceptible to separation), one would expect to see large local concentrations of OH*, because of the much-increased residence time. The lack of such features indicate that, in this case, it is most likely thermal choking that is leading to the development of the unsteady flow phenomena.

In figure 12 is shown a similar sequence of images close to the injector for ER=0.7. In this case, the plotted levels of OH* have been normalized in each image so that the levels are no longer consistent between different images (but are consistent within a given image); this was done in order that the interaction between the flow and combustion features at a given time could be better discerned in earlier images. In the first image (t=3.3 ms), the shock system has not yet arrived within the visualization window, and the picture is similar to that observed in figures 5 and 6: the penetration of H_2 is now significantly higher than for ER=0.35, but the reflecting injection shock is seen to give rise to combustion near the injector-side wall, as previously. From the second image (t=3.62) onwards, the upstream-propagating system is visible in the visualization window. As in the mid-combustor visualizations, the most prominent flow feature is the shock structure on the cowl-side wall, but now a strong combustion feature (indicated by the red OH* levels) is observed to precede this shock on the injector-side wall. This suggests the presence of a separation bubble on the injector-side wall, evidence of which is also seen in some of the Schlieren images (the image taken with the continuous light source in figure 4 gives perhaps a better indication of this than those taken with the laser, as the instantaneous turbulent structures in the latter obscure the picture slightly). This separation must be considered a by-product of the unstart process, rather than a cause, however. The shock train continues moving upstream, but from approximately 4.6 ms, appears to find a quasi-stable configuration, with the cowl shock lodging at roughly x=85 mm, approximately 3 duct heights downstream of the injector. This is consistent with the pressure measurements in figure 9. The main combustion zone is then fixed immediately behind the impingement point of this shock on the injector-side wall, and highly separated flow appears to be present in this region. Following the conclusion of the test time, the increasing equivalence ratio causes the shock structure to again move upstream, and fully subsonic flow is observed in the final image at 6.94 ms.

The development of the transient flow phenomena for ER=0.7 has been seen to typically begin before the establishment of what would normally be considered the steady test time from 3.5-6.0 ms. However, it has also been noted the flow is typically established and has roughly attained its test-time value by 2.5 ms; furthermore, we are more concerned here with providing a qualitative description of the transient phenomena, rather than trying to predict, for example, the exact equivalence ratio at which combustor unstart will occur. To show that the development observed for ER=0.7 is a general feature of the unstart in the HyShot II configuration, in figure 13 are shown Schlieren images from the mid-combustor at the beginning of the transient phase in each case for equivalence ratios of 0.53, 0.7 and 1.1. The same flow features are observed to be present in all cases (although only the first shock in the train is visible for the highest equivalence ratio, the following shocks were visible in subsequent images), in spite of the quite different times in the development of the wind tunnel flow. Note also that this suggests the same mechanism, i.e., thermal choking, to be responsible for the unsteady flow development in all of these cases.

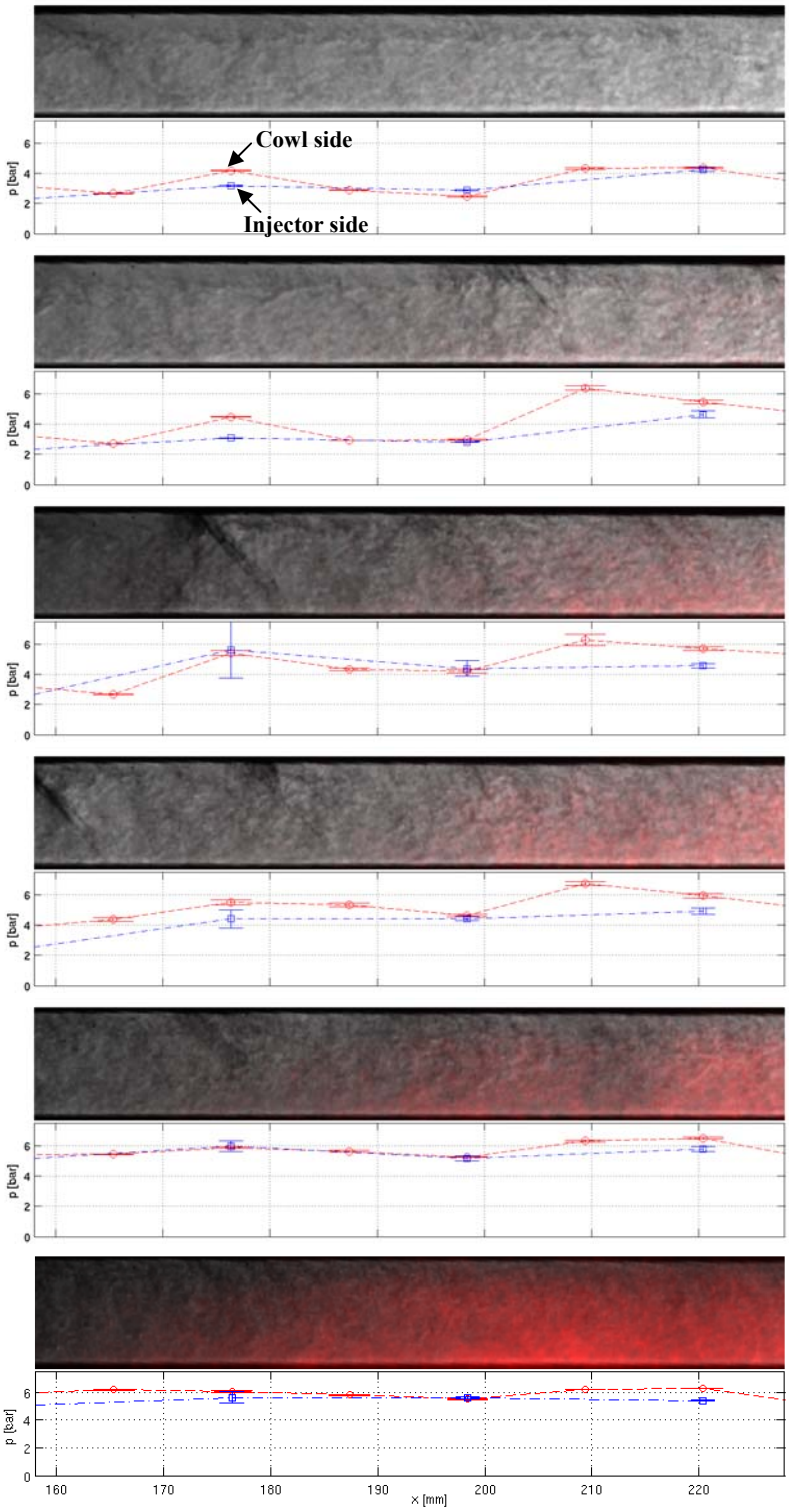

Figure 11: Unsteady development of combustor flow in the rear-central chamber for ER=0.7, showing composite Schlieren/OH* images, together with measured pressures on the injector-side (red) and cowl-side (blue) walls, at times (top to bottom) 2.34, 2.63, 2.85, 2.98, 3.30, 3.81 ms from shock reflection. Injection is on the lower wall (at x=58 mm) in the images.

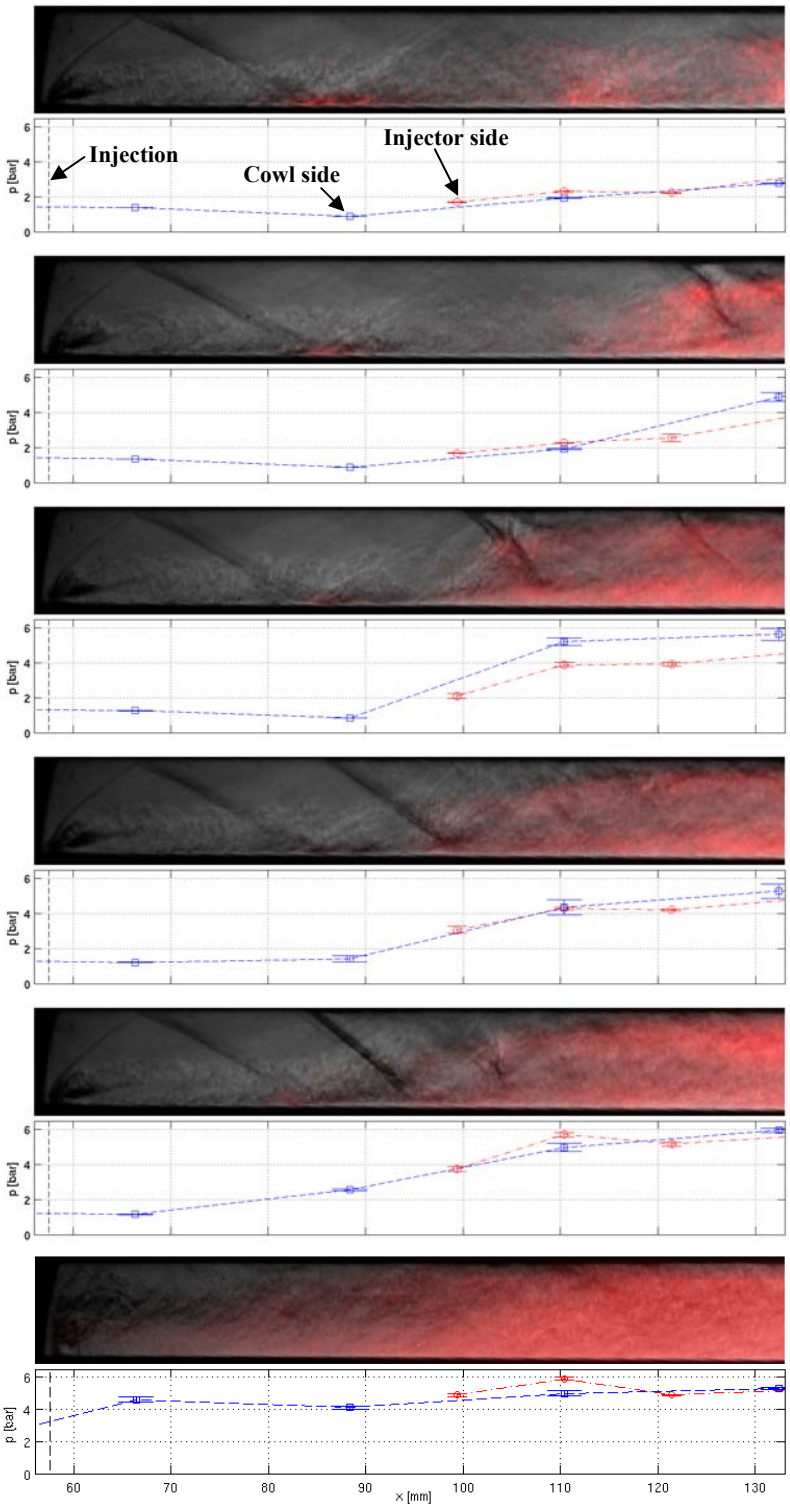

Figure 12: Unsteady development of combustor flow near the injector for ER=0.7, showing composite Schlieren/OH* images, together with measured pressures on the injector-side (red) and cowl-side (blue) walls, at times (top to bottom) 3.30, 3.62, 4.26, 4.58, 5.86, 6.94 ms after shock reflection.

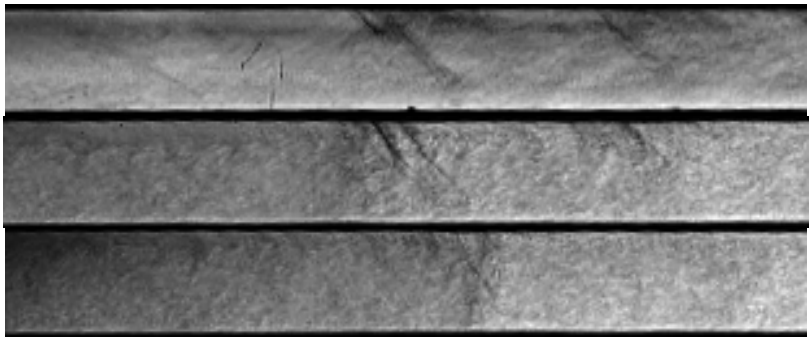

Figure 13: Schlieren images of the developing unsteady shock train for (top to bottom) ER = 0.53 at 7.3 ms, ER=0.7 at 2.9 ms, and ER=1.1 at 2.1 ms.

As mentioned earlier, the pressure of the injected hydrogen remains approximately constant over a period of ~50 ms, whereas the reservoir pressure continually decreases after the conclusion of the steady test time; thus, the effective equivalence ratio increases. In all combustion experiments, at some point following the termination of the test time, large-scale pressure oscillations were observed inside the combustion chamber. For ER=1.1, the establishment of these oscillations occurred as early as 8 ms after shock reflection, while for lower equivalence ratios this occurred later. From figure 2, the flow has not yet been contaminated by driver gas at 8 ms, so it is still possible to draw valid conclusions about the combusting flow at this point in time. Figure 14 shows one example of these pressure oscillations: the unsteady equivalence ratio is plotted here together with a time-resolved pressure trace on the injector side wall for a (steady) equivalence ratio of 1.1. The high-amplitude oscillations from roughly 8 ms are similar to those observed by, for example, Wagner et al.[3] and Tan & Guo[2] for an unstarted inlet (often referred to as "buzzing"). At the onset of the oscillations, the effective equivalence ratio has risen to approximately 1.35; values between 1.35 and 1.45 were found to be typical. The oscillation frequency here is almost exactly 1 kHz: together with an average sound speed, a, of approximately 1100 m/s in the duct (estimated from a TAU computation), this gives a normalized frequency $f^*=fL/a$ (where L is the duct length) of approximately 0.27. This is somewhat higher than the value of 0.11 obtained by Wagner et al.[3] (note that the use of the static rather than the stagnation sound speed makes little difference for subsonic flows – a maximum discrepancy of 9% results), but in the present geometry the open duct ends mean that the chamber may act more like a half-wave resonator than the quarter-wave resonator suggested to be more appropriate for the earlier study (due to their use of a deflecting plate at the duct exit). Thus, normalized frequencies approximately double those of Wagner et al. might be expected, and this is roughly what is observed here.

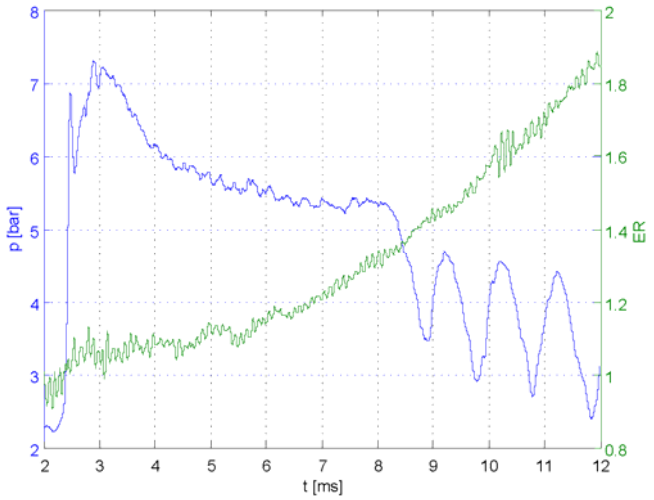

Figure 14: Pressure trace within the combustion chamber showing the high-amplitude oscillations present from approximately 8 ms, plotted together with the unsteady equivalence ratio.

VI. Conclusions

A set of experiments has been carried out in the HEG facility with a particular emphasis on investigating the transient phenomena present in the HyShot II combustor under high equivalence-ratio conditions. In addition to surface pressure measurements on the injector- and cowl-side walls, flow visualization in the form of pulsed-diode laser Schlieren and OH* chemiluminescence was carried out. While the two types of visualization could not be obtained simultaneously in a single run, a comparison of pressure measurements between runs allowed the correlation of the obtained Schlieren and OH* images. The Schlieren images revealed that the "unstart" process here begins with the development of a shock train in the central to rear combustion chamber that subsequently propagates upstream; the speed of this propagation was found from pressure measurements to vary strongly with equivalence ratio. OH* visualizations did not suggest the presence of strong separation features with the formation of this shock train, indicating that the unstart process is initiated by thermal choking; however, a separation bubble was observed to form on the injector-side wall when the shock train had moved further upstream. For ER=0.7, the shock system was observed to lodge on the cowl-side wall approximately 3 duct heights downstream of the injection position.

Acknowledgments

This work was performed within the "Long-Term Advanced Propulsion Concepts and Technologies II" project investigating high-speed transport. LAPCAT II, coordinated by ESA-ESTEC, is supported by the EU within the 7thFramework Program, Theme 7 TRANSPORT, Contract no.: ACP7-GA-2008-21 1485. Further info on LAPCAT II can be found on **http://www.esa.int/techresources/lapcat_II**.

References

[1]Wieting, A. R., "Exploratory Study of Transient Unstart Phenomena in a Three-Dimensional Fixed-Geometry Scramjet Engine", NASA TN D-8156, March 1976.

[2]Tan, H.-J., Guo, R.-W., "Experimental Study of the Unstable-Unstarted Condition of a Hypersonic Inlet at Mach 6", *Journal of Propulsion and Power*, Vol. 23, No. 4, 2007.

[3]Wagner, J.L., Yuceil, K.B., Valdivia, A., Clemens, N.T., Dolling D.S., "Experimental Investigation of Unstart in an Inlet/Isolator Model in Mach 5 Flow", *AIAA Journal*, Vol. 47, No. 6, 2009.

[4]Shimura T., Mitani, T., Sakuranaka, N., Izumikawa, M., "Load Oscillations Caused by Unstart of Hypersonic Wind Tunnels and Engines", *Journal of Propulsion and Power*, Vol. 14, No. 3, 1998.

[5]O'Byrne, S., Doolan, M., Olsen, S.R., Houwing, A.F.P., "Analysis of Transient Thermal Choking Processes in a Model Scramjet Engine", *Journal of Propulsion and Power*, Vol. 16, No. 5, 2000.

[6]Paull, A., Alesi, H., Anderson, S., "The HyShot flight program and how it was developed," *AIAA/AAAF 11th International Space Planes and Hypersonic Systems and Technologies Conference*, Orleans, France, 2002.

[7]Gardner, T., Hannemann, K., Paull, A., Steelant, J., "Ground Testing of the HyShot supersonic combustion flight experiment in HEG", *Proceedings of the 24th International Symposium on Shock Waves*, Beijing, 2004.

[8]Hannemann, K., Karl, S., Martinez Schramm, J., Steelant, J., "Methodology of a combined ground based testing and numerical modelling analysis of supersonic combustion flow paths", *Shock Waves* (online), Springer, 2010

[9]Hannemann, K., Schnieder, M., Reimann, B., Martinez Schramm, J., "The influence and delay of driver gas contamination in HEG", *21st AIAA Aerodynamic Measurement Technology and Ground Testing Conference*, Denver, CO, 19-22 June, 2000

[10]Hannemann, K., "High Enthalpy Flows in the HEG Shock Tunnel: Experiment and Numerical Rebuilding", 41st AIAA *Aerospace Sciences Meeting and Exhibit*, 6-9 Jan, Reno, Nevada, 2003

[11]Najm, H.N., Paul, P.H., Mueller, C.J. Wyckoff, P.S., "On the Adequacy of Certain Experimental Observables as Measurements of Flame Burning Rate", *Combustion and Flame*, Vol. 113, 1998, pp.312-332

[12]Haber, L.C., Vandsburger, U., "A Global Reaction Model for OH* Chemiluminescence Applied to a Laminar Flat-Flame Burner", *Combustion Science and Technology*, Vol. 175, 2003, pp.1859-1891.

[13]Gerhold, T., Friedrich, O., Evans, J., Galle, M., "Calculation of Complex Three-Dimensional Configurations Employing the DLR-TAU-Code", AIAA-Paper 97-0167, 1997